

# **Selection of Processing Parameters in Laser Microwelding. Part 1: Continuous Wave (CW) Mode**

J. COROADO\*, S. GANGULY, W.J. SUDER, S. WILLIAMS, S. MECO AND  
G. PARDAL

*Welding Engineering and Laser Processing Centre, Cranfield University, Cranfield, Bedfordshire,  
MK43 0AL, UK*

A phenomenological model which specifies the penetration depth and width of the fusion zone in laser microjoining can be a very useful tool in achieving the required welding parameters for a desired application. In this study the power factor model, previously established and validated in macrowelding, has been tested in fibre laser microwelding, enabling achievement of a particular weld independently of a laser system. Different weld profiles in aluminium and stainless steel were correlated with various combinations of parameters for a wide range of beam diameters. It has been shown that the same penetration depth can be achieved with different weld profiles. A similar trend, as previously found in macrowelding, has been confirmed in microwelding. It was demonstrated that the depth of penetration can be kept constant independently of the laser system until certain limit of beam size.

*Keywords: Fibre laser, 5251 aluminium alloy, 304L stainless steel, laser microwelding, interaction time, depth of penetration, beam diameter, weld shape, power factor model*

## **1 INTRODUCTION**

In industrial production of electronic components, devices and accessories, the development towards micro-scale components is leading to the integration of high precision and high performance joining techniques, which can

---

\*Corresponding author: E-mail: julio.coroado@gmail.com

ensure good quality of the final product. Microwelding, normally requires strong joints with good esthetical appearance, good resistance to corrosion and durability [1]. The high beam quality of single mode fibre lasers allows them to be narrowly focused on the material surface, leading to a high beam energy density and consequently to small thermal input and small heat affected zone (HAZ), which makes the fibre lasers a perfect tool for micro-joining applications [2]. As the thickness of the joining parts decreases, the likelihood of distortion increases. To enable miniaturization and enhance functionality of electronic components, the welding distortion and thermal foot print have to be minimised [3], which can be only done through a precise control of the heat input [4]. Generally, pulsed wave laser is used in micro-joining [5] but also continuous wave (CW) mode can be utilized for such application [6]. The high beam quality and flexibility of lasers enable a fully automated and reliable manufacturing process [7].

The great flexibility in terms of energy density delivered to the work piece, which can be precisely controlled by the size and shape of the beam, axially [8] and radially [9], and also by different combinations of laser output power and travel speed. Many parameters have a significant influence on the flow dynamics of the weld pool during the process [8-9] affecting, the quality and final shape of a joint; that is, the depth of penetration and weld width [11]. Several studies have been performed to analyse the keyhole's behaviour during its formation based on acoustic [12], thermal and visual [13] and online-X-ray [14] monitoring. Short laser-material interaction time and high power density increases the turbulence in the melt pool, leading to spatter and melt ejection [15], whereas long interaction time increases the heat input in the material, raising this risk of distortion.

The welding parameters are normally optimized based on the trial and error approach, which means the process is specific to a particular laser system, with a unique beam diameter. When transferred to another system with different optical arrangement, normally a new set of parameters needs to be developed which is time consuming and expensive. Some studies have been performed in order to define the weld profile independently of the laser system used, based on energy absorption [16], dimensionless numbers [4] and physical properties of the material [17]; nevertheless, only general trends could be established rather than accurately predict a set of defined processing parameters for a certain welding application. Jaehun *et al.* [6] studied the effect of beam diameter on the weld profile in laser microjoining. They found that small beams are preferred since for larger beams, the surface tension is unable to sustain a stable weld pool. Also, the tensile strength of the joints tested was inversely proportional to the penetration depth, which was related to the overheating of the thin foils for deeper penetration., Such studies, however, provide optimum joining conditions for a specific system only. Suder and Williams [18] created a system of parameters which specify the welding conditions independently of the laser system through the power factor model.

The model has been developed only for keyhole mode, as the laser absorptivity by the material changes with the welding mode: conduction; keyhole; and mixed mode [8, 17]. It gives the optimal laser conditions in terms of laser power and travel speed for a given beam diameter, to obtain a specific weld profile. It was tested first in low carbon steel and titanium alloys [18] and further extended to aluminium alloy [19]. The model can be used to find a particular weld width and a desirable penetration depth for a particular application, independently of the laser system used, simplifying and improving the transferability of the system parameters without the need for repeated approach. However, these studies were focused on macrowelding in 12 mm thick plates primarily, involving high energy levels applied in large beam diameters, which is not suitable for microprocessing. Andreas *et al.* [20] tested the power factor in thin stainless steel foils but the correlation between power factor and interaction time was only to generate a full penetration weld and not to predict the evolution of weld profile.

In laser microjoining the ratio between the beam diameter and the material thickness can be much smaller as compared to macrowelding, which usually results in higher power density applied. In this study, a correlation between laser output power, travel speed and beam diameter and the formation of welded joint is investigated and outcome used to develop an analytical model for parameter selection for a specific application.

## 2 DEFINITION OF POWER FACTOR

In the traditional approach the laser system parameters used are laser output power,  $P_L$ , welding speed,  $v$ , and beam diameter,  $d$ . The last one is often even disregarded, which may cause non-reproducible results in different optical setups. The fundamental laser material interaction parameters (FLMIP) are the power density,  $q_p$ , interaction time,  $t_i$  and specific point energy,  $E_{SP}$ , and are introduced to overcome this problem since they can characterize the laser welding process uniquely based on the energy received by the material [21]. Power density is calculated as the ratio of laser output power to the area of laser spot on the surface,  $A_S$ , as given by:

$$q_p = \frac{P_L}{A_S} \quad (1)$$

The interaction time is defined as the ratio of beam diameter to welding speed:

$$t_i = \frac{d}{v} \quad (2)$$

The specific point energy is defined as the energy delivered within a laser spot. It is equal to the product of power density, interaction time and the laser spot area on the material's surface, as given by:

$$E_{SP} = q_p t_i A_S = \frac{P_L d}{v} \quad (3)$$

From Equation (3) can also be derived the energy density,  $E_D$ , which corresponds to the specific point energy divided by the area of the spot size:

$$E_D = \frac{E_{SP}}{A_S} \quad (4)$$

It was already proven that the depth of penetration for a given interaction time, is proportional to the product of power density and beam diameter [21]. Later, this product was defined as the power factor,  $P_F$  [18], which also corresponds to the ratio of laser power to the beam diameter, as given by

$$P_F = q_p d = \frac{P_L}{d} \quad (5)$$

### 3 EXPERIMENTAL DETAILS

#### 3.1 Materials specifications

To investigate which parameters control the weld bead profile in laser microwelding a set of bead on plate welds was done in 5251 aluminium alloy and austenitic stainless steel 304L. Their chemical composition are shown in Table 1 and Table 2, respectively.

TABLE 1  
Chemical composition (wt.%) of the 5251 aluminium alloy used in this work.

Si	Fe	Cu	Mn	Mg	Zn	Ti	Cr	Al
Max 0.4	Max 0.5	Max 0.15	0.1 to 0.5	1.7 to 2.4	Max 0.15	Max 0.15	Max 0.15	Bal.

TABLE 2  
Chemical composition (wt.%) of 304L austenitic stainless steel used in this work.

Si	S	C	P	Mn	Ni	N	Cr	Fe
Max 1.00	Max 0.02	Max 0.03	Max 0.05	Max 2.00	8.00 to 10.50	Max 0.11	17.50 to 19.50	Bal.

### 3.2 Experimental procedure

A 500 W output power CW single mode fibre laser (redPOWER cube; SPI Lasers) with 1070 nm wavelength was used in this study. The laser beam was delivered through an optical fibre of 50  $\mu\text{m}$  and collimated with an 80 mm focal length lens. The fibre was connected to a galvo-scanner (Super-scan II; Raylase, GmbH) with a F160 theta lens. Properties of the laser beam such as beam diameter, focus position and divergence angle were measured using a slit scan beam profiler (Beam'R2; DataRay, Inc.). All beams exhibited a Gaussian intensity distribution. The laser output power was measured by a power meter (D40-HPB; Laserpoint SRL). The welding process was conducted out of the focal point in all experiments, i.e. with the laser beam defocused on the surface of the material, as shown in Figure 1.

The effect of interaction time and power factor on the penetration depth has been investigated in a set of bead-on-plate welds with different beam diameters of 35, 59 and 89  $\mu\text{m}$ . For each beam, different combinations of laser power and travel speed were used, producing a range of interaction times from 0.01 to 50 ms and a power factors from 1.7 to 13.8 MW/m, according to Equation (2) and Equation (5), respectively. The set of parameters used in both aluminium and stainless steel is shown in Table 3. The weld shape in terms of depth of penetration and weld width was measured for all of experiments performed. The combination of parameters from Table 3 produced a wide range of combinations of interaction times and power factors for each spot size. Only some examples of how a constant set of power factor and interaction time is transferred between different beam diameters are shown in Table 4.

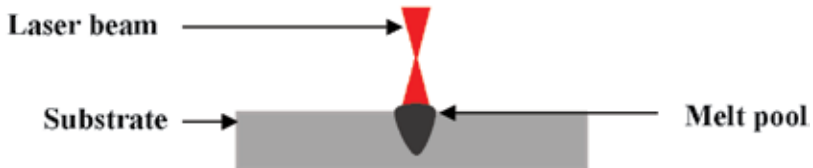


FIGURE 1

Schematic representation of a bead on plate weld with the laser beam defocused on the material surface.

TABLE 3

Set of parameters used for different combinations of interaction time and power factor.

Beam diameter ( $\mu\text{m}$ )	Power (W)	Travel Speed (mm/s)	Interaction time (ms)	Power Density ( $\text{MW}/\text{cm}^2$ )	Specific Point Energy (mJ)	Power Factor ( $\text{MW}/\text{m}$ )
35	58 to 472	2.0 to 3218	0.01 to 13.8	6.0 to 52	2.0 to 4000	1.7 to 13.8
59	195 to 439	6.0 to 1366	0.05 to 50	6.0 to 14	20 to 2771	3.1 to 7.8
89	396 to 494	11 to 1756	0.05 to 8.0	6.0 to 8.0	20 to 3950	4.5 to 5.6

TABLE 4

The laser microwelding parameters calculation for a beam diameter of 35, 59 and 89  $\mu\text{m}$  and different combinations of power factors and interaction times.

Beam Diameter ( $\mu\text{m}$ )	Power Factor (MW/m)	Interaction Time (ms)	Power [W]	Travel Speed (mm/s)	Power Density (MW/cm <sup>2</sup> )	Specific Point Energy (mJ)
35	5.6	0.125	195	280	20	24
59	5.6	0.125	328	472	12	41
89	5.6	0.125	495	712	8	62
35	5.6	1.000	195	35	20	195
59	5.6	1.000	328	58	12	328
89	5.6	1.000	495	88	8	495
35	4.1	0.125	144	280	15	18
59	4.1	0.125	242	472	9	30
89	4.1	0.125	365	712	6	46
35	4.1	1.000	144	35	15	144
59	4.1	1.000	242	58	9	242
89	4.1	1.000	365	88	6	365

### 3.3 Sample analysis procedure

The samples were cut with the following dimensions:  $70 \times 35 \times 2$  mm. In order to measure the depth of penetration and weld width, all welds were cross-sectioned, polished and examined under an optical microscope (LSM 900; Carl Zeiss AG). Keller's solution was applied to etch the welds and reveal the microstructure of aluminium, whereas stainless steel was electrolytically etched with 10% of oxalic acid. Image analysis software (Carl Zeiss Axio Vision 4.8 [22]) was used to measure and determine the weld width and depth of penetration from the micrographs. The depth of penetration measured considers the distance between the material surface and the bottom of the fusion zone. All the samples were cross-sectioned in two different positions and the experimental error was calculated based on the difference of the penetration depth observed between the first and second position.

## 4 RESULTS AND DISCUSSION

### 4.1 Effect of interaction time and power factor on the weld profile for stainless steel

In Figure 2 and Figure 3, depth of penetration is presented as a function of power factor and interaction time using different beams. Constant penetration is demonstrated in stainless steel for constant interaction times but only for

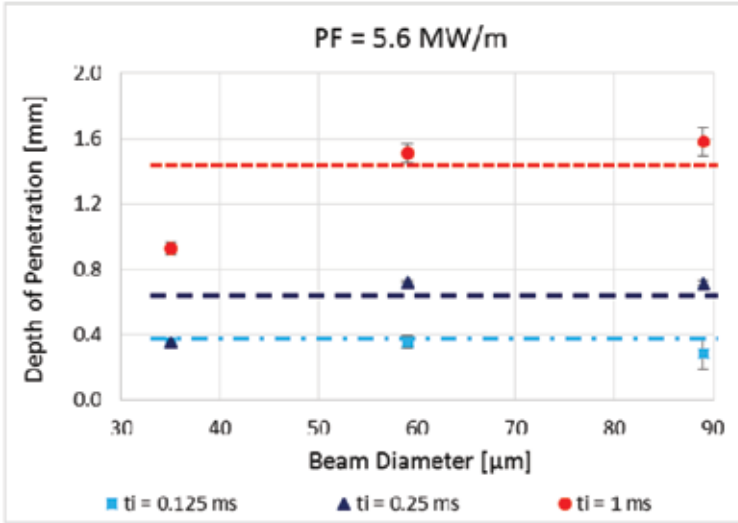


FIGURE 2

Graph showing the effect of the beam diameter on the depth of penetration of CW processing of stainless steel at different interaction times and a constant power of 5.6 MW/m.

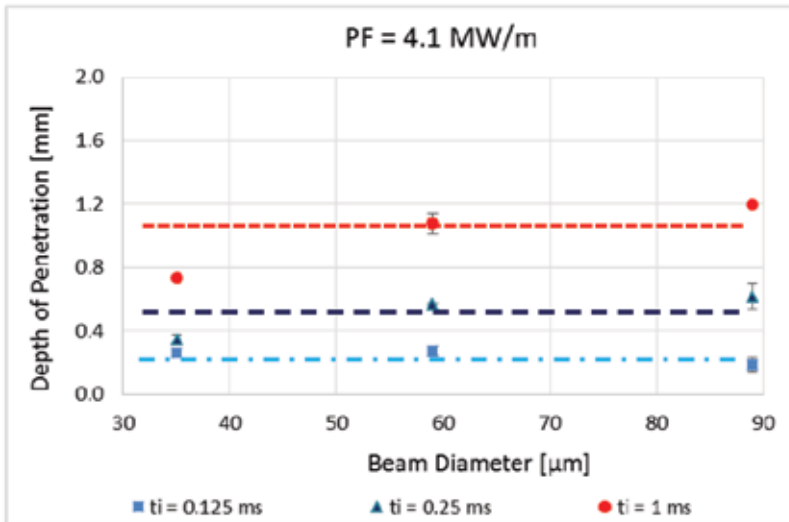


FIGURE 3

Graph showing the effect of the beam diameter on the depth of penetration of CW processing of stainless steel at different interaction times and a constant power of 4.1 MW/m.

certain spot sizes, below which there is discrepancy. For a beam diameter of 35  $\mu\text{m}$ , at 0.25 ms the depth of penetration is lower as in comparison when larger beams of 59 and 89  $\mu\text{m}$  were used, being this discrepancy even more

evident for a longer interaction time of 1 ms. These results are opposite from the previous results demonstrated in macrowelding of low carbon steel [18] and aluminium [19], where the penetration was always constant for all the experimental conditions; however, for the shortest interaction time of 0.125 ms, there is no variation in the depth of penetration.

In microwelding it seems that there is a threshold of the size of the heat source applied in the material's surface to maintain steady state keyhole. It has been observed that the depth of penetration decreases when the beam diameters are reduced at constant processing conditions [21]. The plateau effect observed for small beam diameters can be related to the higher power densities, which attenuates the laser beam in the vapour plume [23] or a strong closing force of the surface tension due to the narrow diameter of keyhole [24]. This phenomena can also be attributed to the laser absorption rate. It is known that the absorption rate in laser welding is affected by the beam diameter and other processing parameters. At low laser power and fast processing speeds, the beam diameter can be partially irradiating the keyhole, reducing the vapour pressure and consequently, the penetration depth [24].

Power density and specific point energy are responsible to control the penetration depth and there is a trade-off between them to keep the penetration depth constant [25]. Both parameters can also be correlated through the energy density. The effect of energy density for a constant power density of 15 MW/cm<sup>2</sup> achieved for a beam diameter of 35 µm in shown in Figure 4. A parabolic

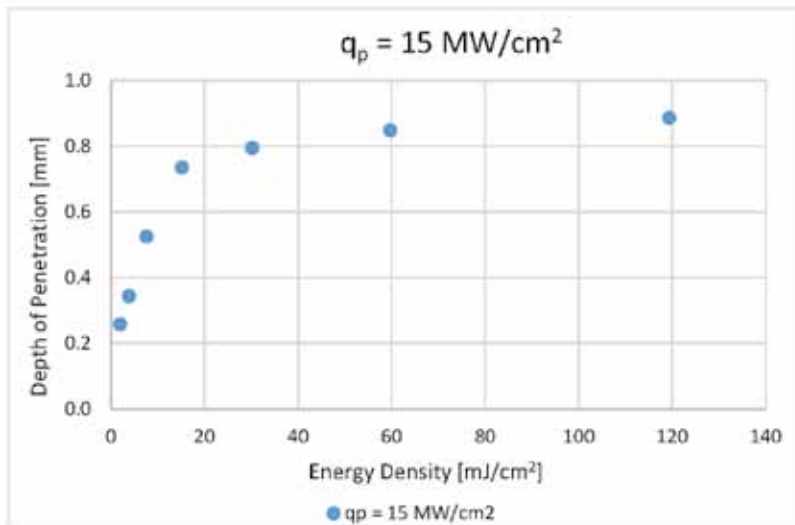


FIGURE 4

Graph showing depth of penetration as a function of energy density for constant power density of 15.3 MW/cm<sup>2</sup> achieved with beam diameters of 35 µm.

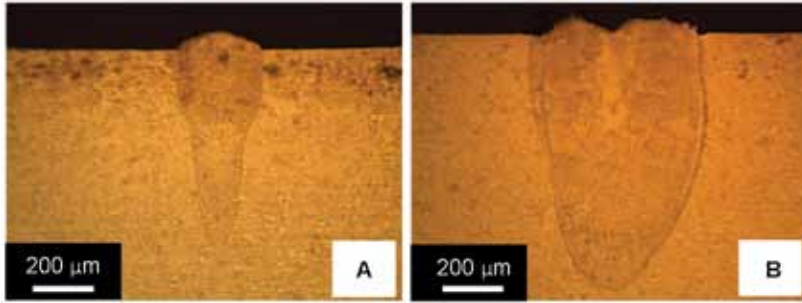


FIGURE 5

Optical micrographs from the CW laser microwelding of stainless steel at constant power density of  $15 \text{ MW/cm}^2$ , laser beam diameter of  $35 \mu\text{m}$  and (a) Energy density of  $30 \text{ mJ/cm}^2$  and (b) Energy density of  $60 \text{ mJ/cm}^2$ .

dependence of energy density on the depth of penetration can be seen. At low energy level there is not much heat available to compensate for conduction losses and maintain the melt pool and keyhole, hence the response of penetration to energy density is low in this region. Increasing the energy density, the penetration depth increases and the keyhole mode is evident, as observed in the correspondent micrograph from Figure 5(a). On the other hand, increasing energy, the thermal gradient in the substrate saturates very quickly for small spot sizes, resulting into enlargement of overall weld pool area without relevant further increase in penetration, as observed in Figure 5(b). So in this region, only an increase of power density can have a significant increase on the vapour pressure and consequently on the penetration [21]. Ayoola *et al.* [26] found that the ratio of energy for conduction losses to the energy for melting increases for small beam diameters, which explains the high cooling effect that the small beam of  $35 \mu\text{m}$  is subjected to maintain a large melt pool and the consequent discrepancy in penetration depth to the larger beams at high interaction time, as previously observed in Figure 2 and Figure 3.

Figure 6 shows all the weld profiles obtained using power factor of 5.6 and  $4.1 \text{ MW/m}$  for different beam diameters and interaction time, which were shown in Figure 2 and Figure 3. Comparing Figure 6(b) and Figure 6(c) with Figure 6(e) and Figure 6(f) it can be concluded that for a constant power factor of  $5.6 \text{ MW/m}$ , increasing the interaction time from 0.125 to 0.250 ms, the depth of penetration depth increases from 0.4 to 0.7 mm and the weld width also increases from 0.11 to 0.16 mm. According to Equation (3), specific point energy is dependent from interaction time, therefore, for longer interaction time, specific point energy is also higher and more penetration can be expected. Decreasing the power factor from 5.6 to  $4.1 \text{ MW/m}$  for a constant interaction time of 1 ms, as shown in Figure 6(h) and Figure 6(i), and Figure 6(k) and Figure 6(l), respectively, the depth of penetration decreased from 1.6 to 1.2 mm.

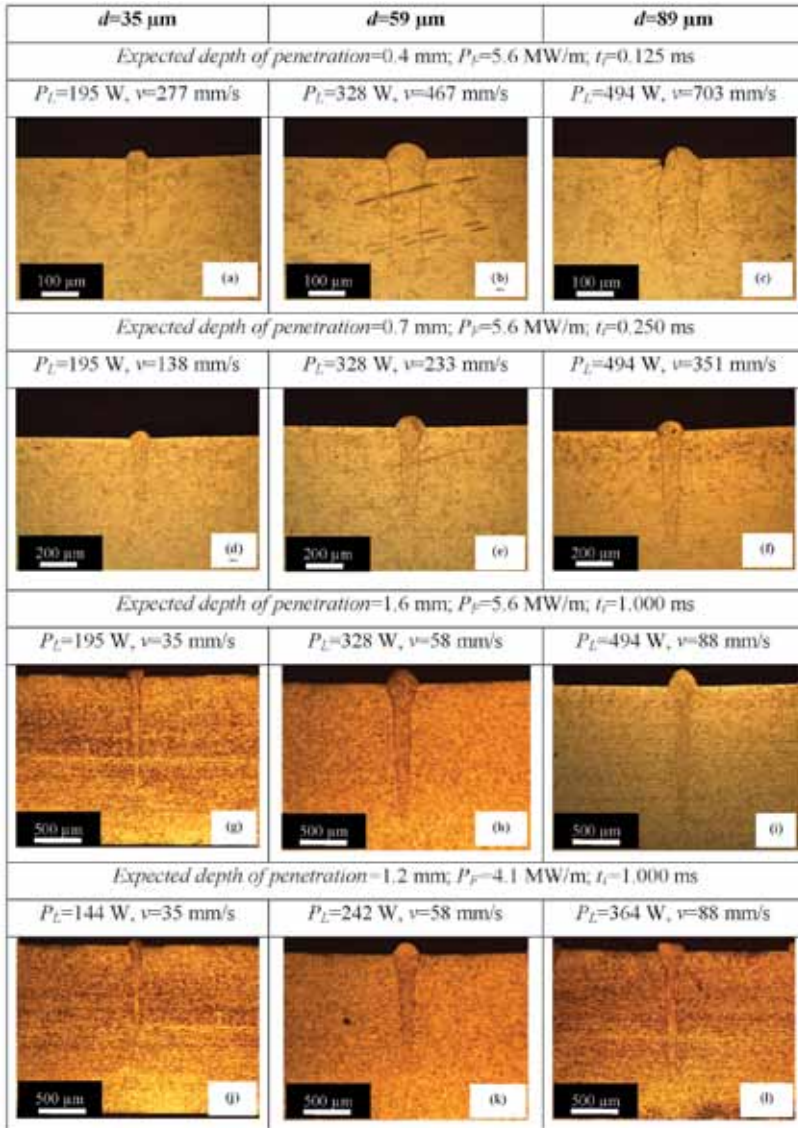


FIGURE 6

Optical micrographs showing constant combinations of power factor and interaction time for different weld depths in CW laser microwelding of stainless steel.

Different combinations of laser power, travel speed and beam diameters were tested to generate different combinations of power factor and interaction time for several depths of penetration. In Figure 7, constant penetration depth curves against interaction time and power factor can be seen. Due to the variation in penetration depth for a spot size of  $35\ \mu\text{m}$ , as previously

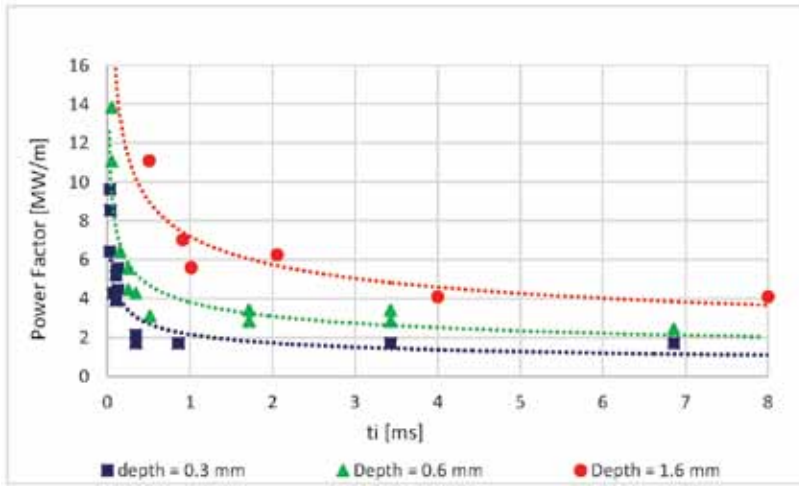


FIGURE 7

Graph showing power factor for depths of penetration of 0.3, 0.6 and 1.6 mm as function of interaction time for beam diameters of 35, 59 and 89  $\mu\text{m}$  in CW laser microwelding of stainless steel.

observed in Figure 2 and Figure 3, this beam diameter was not included in this graph for interaction times above 0.125 ms. A relationship between power factor and interaction time can be observed in laser microwelding, as previously demonstrated in macrowelding using beam diameters 10 $\times$  larger than the ones in this study [18-19]. Some micrographs from the data in Figure 7 are shown in Figure 8. For a constant depth of penetration of 1.6 mm the weld width is narrow for high power factor and short interaction time (see Figure 8(a)) and it becomes wider for longer values of interaction time and lower values of power factor (see Figure 8(c)). These micrographs in Figure 8 emphasize this model as a completely different approach in comparison to the traditional method of parametric study of the welding

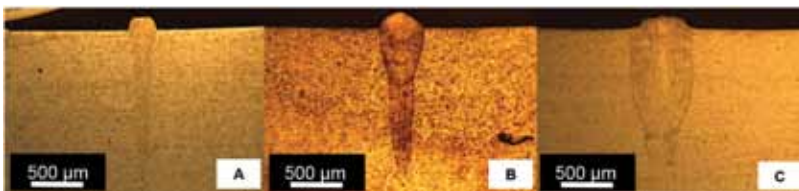


FIGURE 8

Optical micrographs of CW laser microwelds of stainless steel at constant depth of penetration of 1.6 mm achieved with (a) power factor of 11 MW/m and interaction time of 0.5 ms, (b) power factor of 6.1 MW/m and interaction time of 2.1 ms, and (c) power factor of 4 MW/m and interaction time of 8 ms.

parameters selection, which is most of the times based on trial and error and is limited in terms of the capacities of the laser system. Based on a combination of power factor and interaction time, the model allows the user to obtain a certain weld shape for a desired application. For shorter interaction times the process is more productive, since higher travel speed is required for a fixed beam diameter. But, shorter interaction times mean narrower weld width profile, as observed in Figure 8(a), which is not desired for applications where a high fit-up tolerance is necessary. On the other hand, longer interaction times give high fit-up tolerance, as shown in Figure 8(c); however, the productivity is less and the distortions higher and so the necessary laser output power to penetrate a specific material thickness with a certain productivity can be estimated independently of the optical arrangement used.

#### 4.2 Effect of interaction time and power factor on weld profile of aluminium

A similar study to that performed for stainless steel and described in the previous section has also been conducted for aluminium. In Figure 9 and Figure 10, the same three levels of interaction time are correlated with constant power factors of 5.6 and 4.1 MW/m, respectively, for different depths of penetration. Constant trend lines on the depth of penetration are observed in aluminium when the spot size was varied between 35 and 89  $\mu\text{m}$ . For an interaction time of 1 ms, the penetration is less deep for a beam diameter of 35  $\mu\text{m}$ , remaining similar for 59 and 89  $\mu\text{m}$ . In alumin-

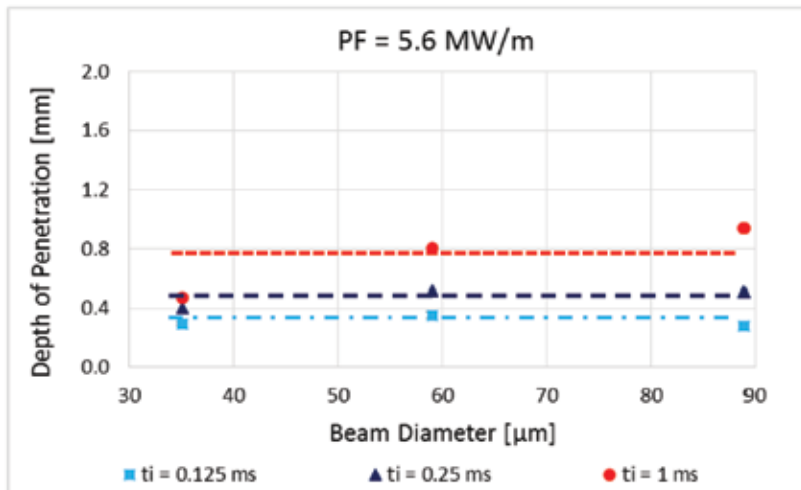


FIGURE 9

Graph showing the effect of the beam diameter on the depth of penetration of CW laser microwelded aluminium at different interaction times and constant power factor of 5.6 MW/m.

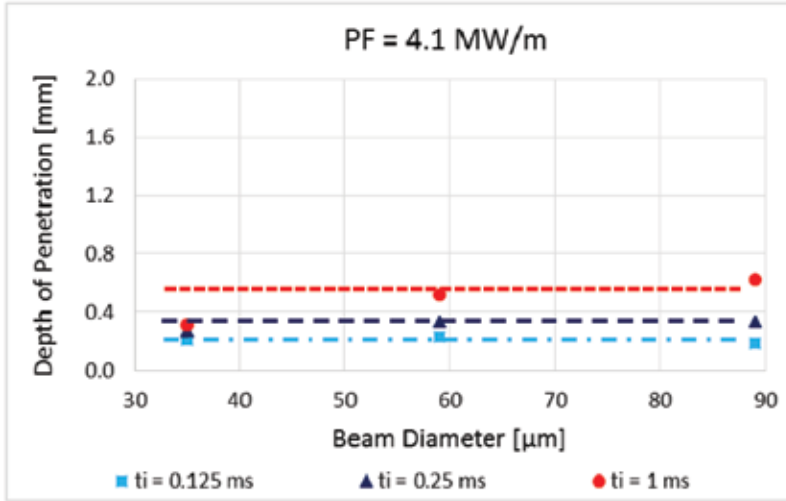


FIGURE 10

Graph showing the effect of the beam diameter on the depth of penetration of CW laser microwelded aluminium at different interaction times and constant power factor of 4.1 MW/m.

ium, like in stainless steel, there is also a threshold size of the beam where the model works.

The micrographs of the corresponding welding parameters of Figure 9 and Figure 10 are depicted in Figure 11. The conclusions are very similar as observed in stainless steel in the previous section. For a constant power factor of 5.6 MW/m, increasing the interaction time from 0.125 to 0.250 ms, the depth of penetration depth increases from 0.3 to 0.5 mm and the weld width also increases from 0.27 to 0.30 mm, as demonstrated in Figures 11(a-c) and Figures 11(d-f), respectively. Decreasing the power factor from 5.6 to 4.1 MW/m for a constant interaction time of 1 ms, the depth of penetration decreased from 0.9 to 0.6 mm, as shown in Figure 11(h) and Figure 11(i), and Figure 11(k) and Figure 11(l). The average weld width was reduced from 0.57 mm to 0.47 mm, which means the power factor mainly influences not only the depth of penetration but also has some effect on the weld width in aluminium.

In Figure 12 the depths of penetration of 0.3, 0.7 and 1 mm are plotted as a function of power factor and interaction time using beam diameters between 35 and 89  $\mu\text{m}$ . Due to the variation of the penetration depth for a beam diameter of 35  $\mu\text{m}$  and interaction time of 1 ms, as previously observed in Figure 9 and Figure 10, this laser beam was only used below 1 ms. As observed, the trend lines are generated independently of the beam diameter used, which means that the depth of penetration can be determined only based on power factor and interaction time, independently of the optical

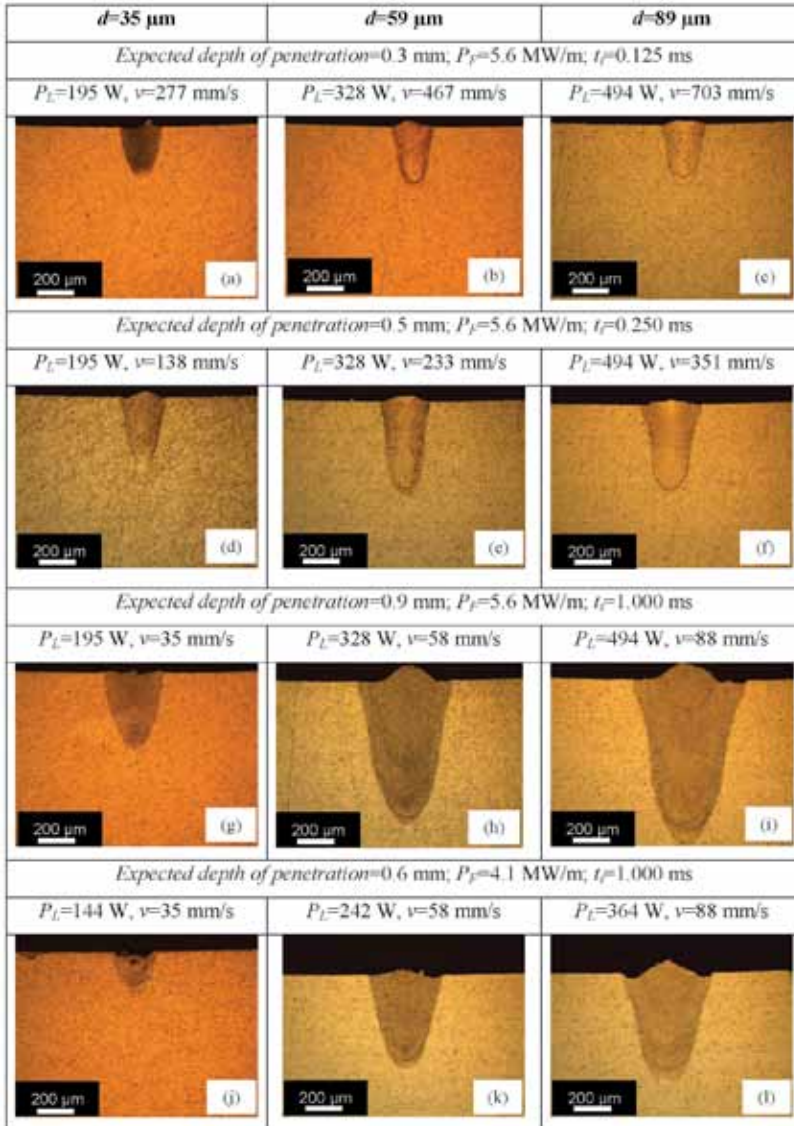


FIGURE 11

Optical micrographs showing constant combinations of power factor and interaction time for different weld depths in CW laser microwelding of aluminium.

arrangement. Some micrographs from the data from Figure 12 are shown in Figure 13. The effect of interaction time on the weld width is visible, with the width increasing with the interaction time. Using this approach, the same weld depth can be achieved with different profiles on different optical arrangements.

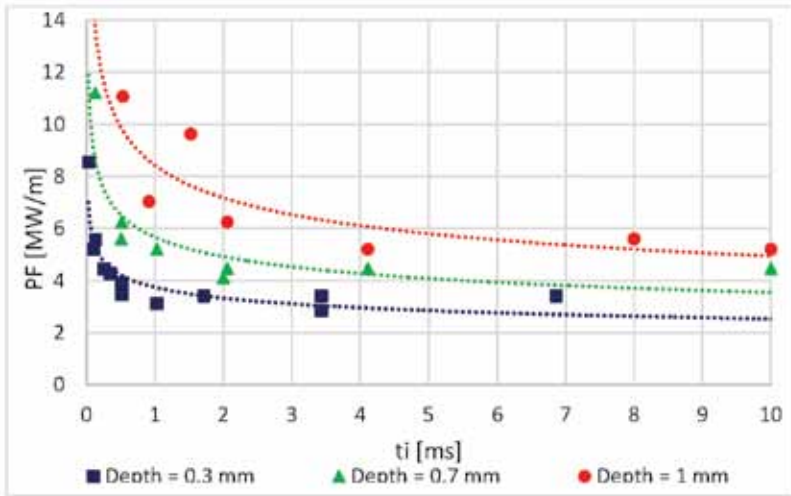


FIGURE 12

Graph of power factor for depths of penetration of 0.3, 0.7 and 1 mm as function of interaction time for laser beam diameters of 35, 59 and 89  $\mu\text{m}$  in CW laser microwelding of aluminium.

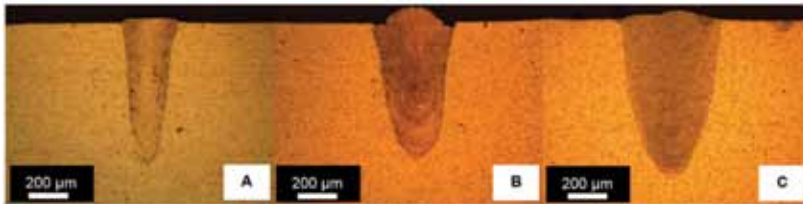


FIGURE 13

Optical micrographs of the CW laser microwelding of aluminium at constant depth of penetration of 0.7 mm achieved with (a) power factor of 11.2 MW/m and interaction time of 0.2 ms, (b) power factor of 4.0 MW/m and interaction time of 2.0 ms, and (c) power factor of 4.5 MW/m and interaction time of 10 ms.

### 4.3 Comparison of power factor model between aluminium and stainless steel

Aluminium and stainless steel are compared in this section for a constant penetration depth of 0.3 mm. The power factor curves were extracted from Figure 7 and Figure 12 and plotted in Figure 14. It is shown that to achieve similar penetration in aluminium, as stainless steel, higher power factor is required in for constant interaction time; that is, the laser output power has to be higher for a fixed beam diameter. On the other hand, at constant power factor, aluminium requires higher interaction time than stainless steel; that is, the necessary travel speed is less for a set beam diameter. One way to com-

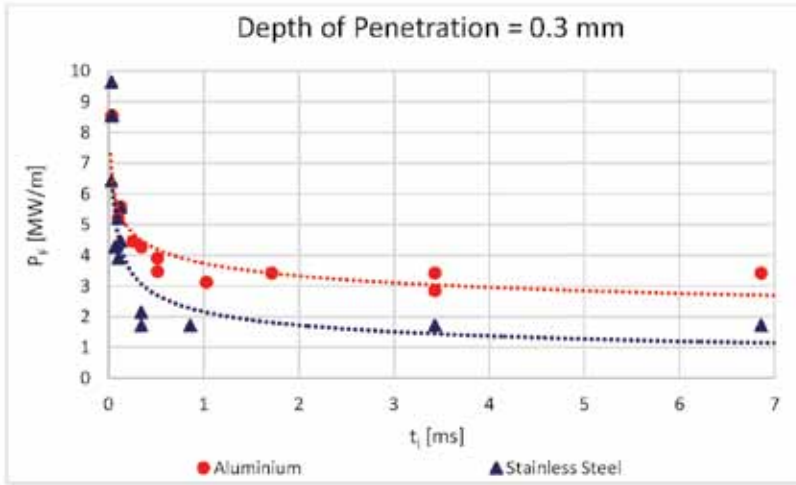


FIGURE 14

Graph showing the comparison of the power factor model trend lines between aluminium and steel for a depth of penetration of 0.3 mm.

pare them is by the characteristic thermal time,  $t_0$ , which measures the time of the thermal diffusivity,  $a$ , over a distance equal to the beam diameter,  $d$  [27], as given by

$$t_0 = \frac{d^2}{16a} \quad (6)$$

The thermal diffusivity measures the rate of transfer of heat of a certain material from a hot to a cold point. For a beam diameter of 35  $\mu\text{m}$ , a thermal diffusivity of  $6 \times 10^{-5} \text{ m}^2/\text{s}$  for aluminium and  $6 \times 10^{-6} \text{ m}^2/\text{s}$  for stainless steel [28-29], the characteristic thermal time of each metal is  $1.35 \times 10^{-6} \text{ s}$  and  $1.39 \times 10^{-5} \text{ s}$ , respectively. This means that in aluminium, the heat takes less time to reach the same distance than in steel, since it is more quickly dissipated in all directions of the substrate; therefore, the temperature rise will be small in aluminium and more power factor is necessary in order to achieve similar penetration as in stainless steel, being the reason why its trend line is above stainless steel in Figure 14.

Some micrographs from Figure 14 are shown in Figures 15(a-c) and Figures 16(a-c) for aluminium and stainless steel, respectively. In Figure 15(a) and Figure 16(a) it can be seen that for the same interaction time, the weld width in aluminium is wider than in steel. Comparing Figure 15(c) and Figure 16(c) the weld width is similar in both metals for an interaction time of 6.8 ms. For longer interaction time and consequently

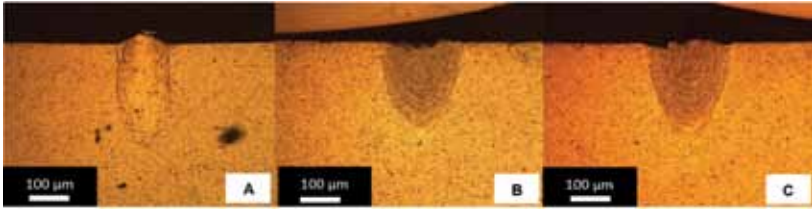


FIGURE 15

Optical micrographs of laser microwelds of aluminium at a constant depth of penetration of 0.3 mm achieved with (a) power factor of 8.5 MW/m and interaction time of 0.2 ms, (b) power factor of 2.8 MW/m and interaction time of 3.4 ms, and (c) power factor of 3.5 MW/m and interaction time of 6.8 ms.

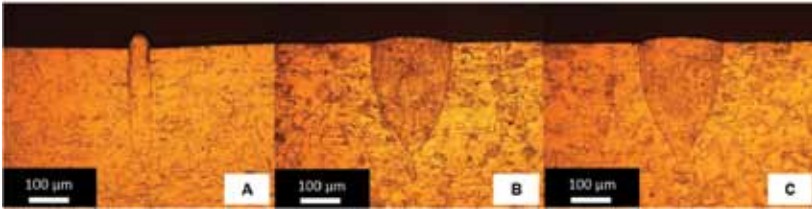


FIGURE 16

Optical micrographs of laser microwelds of stainless steel at a constant depth of penetration of 0.3 mm achieved with (a) power factor of 9.8 MW/m and interaction time of 0.2 ms, (b) power factor of 1.8 MW/m and interaction time of 3.4 ms, and (c) power factor of 1.8 MW/m and interaction time of 6.8 ms.

higher specific point energy, both metals achieve a plateau on the depth of penetration and weld width; nevertheless, this plateau is achieved much sooner in aluminium since the heat is dissipated more efficiently than in stainless steel and the vaporization temperatures are almost the same for both metals [28-29].

## 5 CONCLUSIONS

The power factor model has been used as a predictive algorithm to find the weld profile required for a desired application in laser microwelding of 5251 aluminium alloy and 304L stainless steel. The following conclusions can be drawn from this study:

- (i) As previously observed in macrowelding for mild steel and aluminium, constant penetration depth curves against interaction time and power factor can also be obtained in microwelding for the selection of parameters required for a certain weld width and depth of penetration;

- (ii) In microwelding, the trade-off between power density and specific point energy defines the limits of the power factor model, constraining the applicable size of the beam diameter for a certain interaction time and power factor value, in both aluminium and stainless steel;
- (iii) The smaller characteristic thermal time of aluminium as in comparison to stainless steel justifies the gap in the characteristic curves of power factor vs interaction time in both metals; and
- (iv) The transferability of the power factor model between different optical configurations is possible in microwelding due to the independence from the beam diameter.

## ACKNOWLEDGEMENTS

The researchers would like to acknowledge Innovate UK (TS/MO11089/1) for sponsoring this investigation in the scope of the Environmental Domed End project.

## NOMENCLATURE

$a$	Thermal diffusivity ( $\text{m}^2/\text{s}$ )
$A_S$	Area of the spot size ( $\text{cm}^2$ )
$d$	Beam diameter ( $\mu\text{m}$ )
$E_D$	Energy density ( $\text{J}/\text{cm}^2$ )
$E_{SP}$	Specific point energy (J)
$P_F$	Power Factor (W/m)
$P_L$	Laser output power (W)
$q_p$	Power density ( $\text{MW}/\text{cm}^2$ )
$t_0$	Characteristic thermal time (s)
$t_i$	Interaction time (ms)
$v$	Welding speed (mm/s)

## REFERENCES

- [1] Shi W., Huang J., Xie Y., Li Y. and An F. Laser micro-welding technology for Cu–Al dissimilar metals and mechanisms of weld defect formation. *International Journal of Advanced Manufacturing Technology* **93**(9–12) (2017), 4197–4201.
- [2] Meco S., Pardal G., Ganguly S., Miranda R.M., Quintino L. and Williams S. Overlap conduction laser welding of aluminium to steel. *International Journal of Advanced Manufacturing Technology* **67**(1–4) (2013), 647–654.
- [3] Haglund P., Frostevarg J., Powell J., Eriksson I. and Kaplan A.F.H. Holographic measurement of distortion during laser melting: Additive distortion from overlapping pulses. *Optics & Laser Technology* **100** (2018), 1–6.

- [4] Patschger A., Bliedtner J. and Bergmann J.P. Approaches to increase process efficiency in laser micro welding. *Physics Procedia* **41** (2013), 592–602.
- [5] Ventrella V.A., Berretta J. R. and De Rossi W. Pulsed Nd:YAG laser seam welding of AISI 316L stainless steel thin foils. *Journal of Materials Processing Technology* **210**(14) (2010), 1838–1843.
- [6] Kim J., Kim S., Kim K., Jung W., Youn D., Lee J. and Ki H. Effect of beam size in laser welding of ultra-thin stainless steel foils. *Journal of Materials Processing Technology* **233** (2016), 125–134.
- [7] Ion J. *Laser Processing of Engineering Materials - Principles, Procedure and Industrial Application*. New York: Elsevier. 2005.
- [8] Kaplan A.F.H. Influence of the beam profile formulation when modeling fiber-guided laser welding. *Journal of Laser Applications* **23**(4) (2011).
- [9] Volpp J. and Vollertsen F. Keyhole stability during laser welding - Part I: Modeling and evaluation. *Production Engineering :Research and Development* **10** (2016), 443–457.
- [10] Kim J., Oh S. and Ki H. A study of keyhole geometry in laser welding of zinc-coated and uncoated steels using a coaxial observation method. *Journal of Materials Processing Technology* **225** (2015), 451–462.
- [11] Stavridis J., Papacharalampopoulos A. and Stavropoulos P. Quality assessment in laser welding: a critical review. *International Journal of Advanced Manufacturing Technology* **94**(5-8) (2017), 1825–1847.
- [12] Schou C., Semak V. and McCay T. Acoustic emission at the laser weld site as an indicator of weld quality. *The 13th International Congress on Applications of Lasers and Electro-Optics (ICALEO 1994)*. 17-20 October 1994, Orlando, FL, USA, **41**, pp. 41–50.
- [13] Geiger M., Leitz K. H., Koch H. and Otto A. A 3D transient model of keyhole and melt pool dynamics in laser beam welding applied to the joining of zinc coated sheets. *Production Engineering* **3**(2) (2009), 127–136.
- [14] Boley M., Abt F., Weber R. and Graf T. X-Ray and optical videography for 3D measurement of capillary and melt pool geometry in laser welding. *Physics Procedia* **41** (2013), 488–495.
- [15] Chang B., Blackburn J., Allen C. and Hilton P. Studies on the spatter behaviour when welding AA5083 with a Yb-fibre laser. *International Journal of Advanced Manufacturing Technology* **84**(9-12) (2016), 1769–1776.
- [16] Fuerschbach P.W. and Eisler G.R. Effect of laser spot weld energy and duration on melting and absorption. *Science and Technology of Welding and Joining* **7**(4) (2002), 241–246.
- [17] Assuncao E. and Williams S. Effect of material properties on the laser welding mode limits. *Journal of Laser Applications* **26**(1) (2014), 012008.
- [18] Suder W.J. and Williams S. Power factor model for selection of welding parameters in CW laser welding. *Optics & Laser Technology* **56** (2014), 223–229.
- [19] Coroado J., Meco S., Williams S., Ganguly S., Suder S., Quintino S. and Assuncao E. Fundamental understanding of the interaction of continuous wave laser with aluminium. *International Journal of Advanced Manufacturing Technology* **93**(9-12) (2017), 3165–3174.
- [20] Patschger A., Güpner M., Bliedtner J. and Bergmann J. Remote micro welding with multi-mode and single-mode fiber lasers – A comparison. *The 32nd International Congress on Applications of Lasers & Electro-Optics (ICALEO 2013)*. 6-10 October 2013, Miami, FL, USA, **32**, pp. 805–815.
- [21] Suder W.J. and Williams S. Investigation of the effects of basic laser material interaction parameters in laser welding. *Journal of Laser Applications* **24**(3) (2012), 032009.
- [22] Carl Zeiss Axio Vision. (2019). Retrieved 10<sup>th</sup> January 2019, from <https://www.zeiss.com/microscopy/int/products/microscope-software/axiovision.html>.
- [23] Verhaeghe G. and Hilton P. The effect of spot size and laser beam quality on welding performance when using high-power continuous wave solid-state lasers. *The 24th International Congress on Applications of Lasers and Electro-Optics (ICALEO 2005)*. 31 October – 3 November 2005, Miami, FL, USA, **1**, pp. 264–271.

- [24] Kawahito Y., Matsumoto N., Abe Y. and Katayama S. Relationship of laser absorption to keyhole behavior in high power fiber laser welding of stainless steel and aluminum alloy. *Journal of Materials Processing Technology* **211**(10) (2011), 1563–156.
- [25] Suder W.J. Study of Fundamental Parameters in Hybrid Laser Welding. PhD Thesis, Cranfield University. 2011.
- [26] Ayoola W.A., Suder W.J., and Williams S.W. Parameters controlling weld bead profile in conduction laser welding. *Journal of Materials Processing Technology* **249** (2017), 522–530.
- [27] Ashby M.F. and Easterling K.E. The transformation hardening of steel surfaces by laser beams-I. Hypo-eutectoid steels. *Acta Metallurgica* **32**(11) (1984), 1935-1948.
- [28] Aalco. Aluminium Alloy 5251 - H22 Sheet and Plate properties. (2019). Retrieved 10<sup>th</sup> January 2019, from [http://www.aalco.co.uk/datasheets/Aluminium-Alloy-5251-H22-Sheet-and-Plate\\_150.ashx](http://www.aalco.co.uk/datasheets/Aluminium-Alloy-5251-H22-Sheet-and-Plate_150.ashx).
- [29] Aalco. Stainless Steel - Austenitic - 304L properties. (2019). Retrieved 10<sup>th</sup> January 2019 from, [http://www.aalco.co.uk/datasheets/Stainless-Steel-14301-Sheet-and-Plate-Quarto-Plate--CPP-Plate\\_343.ashx](http://www.aalco.co.uk/datasheets/Stainless-Steel-14301-Sheet-and-Plate-Quarto-Plate--CPP-Plate_343.ashx).